Incomplete reactions in nanothermite composites

Rohit J. Jacob[1], Diana L. Ortiz-Montalvo[2], Kyle R. Overdeep[3], Timothy P. Weihs[3] and Michael R. Zachariah[1,a)]

[1]*Department of Chemical and Biomolecular Engineering and Department of Chemistry and Biochemistry, University of Maryland, College Park, Maryland 20706, USA*
[2]*Materials Measurement Science Division, National Institute of Standards and Technology, Gaithersburg, Maryland 20899, USA*
[3]*Department of Materials Science and Engineering, Johns Hopkins University, Baltimore, Maryland 21218, USA*

ABSTRACT

Exothermic reactions between oxophilic metals and transition/ post transition metal-oxides have been well documented owing to their fast reaction time scales (≈ 10 μs). This article examines the extent of reaction in nano-aluminum based thermite systems through a forensic inspection of the products formed during reaction. Three nanothermite systems (Al/CuO, Al/Bi_2O_3 and Al/WO_3) were selected owing to their diverse combustion characteristics thereby providing sufficient generality and breadth to the analysis. Microgram quantities of the sample were coated onto a fine platinum wire, which was resistively heated at high heating rates (≈ 10^5 K/s) to ignite the sample. The subsequent products were captured/quenched very rapidly (≈ 500 μs) in order to preserve the chemistry/morphology during initiation and subsequent reaction and were quantitatively analyzed using electron microscopy (EM), focused ion beam (FIB) cross-sectioning followed by energy dispersive X-ray spectroscopy (EDX). Elemental examination of the cross-section of the quenched particles show oxygen predominantly localized in the regions containing aluminum, implying the occurrence of redox reaction. The Al/CuO system, which has simultaneous gaseous oxygen release and ignition ($T_{Ignition} \approx T_{Oxygen\ Release}$), shows substantially lower oxygen content within the product particles as opposed to Al/Bi_2O_3 and Al/WO_3 thermites, which are postulated to undergo a condensed phase reaction ($T_{Ignition} << T_{Oxygen\ Release}$). An effective Al:O composition for the interior section was obtained for all the mixtures, with the smaller particles generally showing higher oxygen content than the larger ones. The observed results were further corroborated with the reaction temperature, obtained using a high-speed spectro-pyrometer, and bomb calorimetry conducted on larger samples (≈ 15 mg). The results suggest that thermites that produce sufficient amounts of gaseous products generate smaller product particles and achieve higher extents of completion.

Keywords: *Nanothermite; focused ion-beam milling; product analysis; condensed phase*

a) Author to whom correspondence should be addressed. Electronic mail: mrz@umd.edu

This manuscript was accepted by J. Appl. Phys. Click here to see the version of record.

I. INTRODUCTION

Thermite reactions are exothermic, redox reactions between a metallic fuel and a metal oxide and are known to have high energy density on both gravimetric and volumetric basis[1]. Traditional thermite mixtures, with fuel and oxidizer moieties mixed at the micrometer scale, suffer from significant ignition delay times and poor reaction rates arising from large diffusion length scales and slow conductive heat transfer.[2,3] With the advent of nanotechnology and the subsequent improvement of control at the nanoscale, researchers showed two decades ago that an enhanced reactivity could be observed when the fuel and oxidizer were mixed at the nanoscale[4] and coined the term metastable intermolecular composites (MIC) for such systems. MICs have shown tremendous improvement in reaction rate[5] and with sufficient tuning of the microstructure and composition, have been shown to approach propagation rates as high as 2500 m/s in burn tube measurements.[6,7]

One of the most attractive aspects of MICs is the tunability that allows the use of different metal/ metal-oxide combinations, custom nanostructures[7,8] and production techniques.[9,10,11] Several studies have been undertaken to mechanistically explain the combustion of MICs.[12,13] Heat transfer is considered to be dominated by convection and molten particle advection,[14,15] corroborated by the observation of peak reactivity in cases with highest gas production. The initiation may undergo a condensed phase mechanism where the fuel and oxygen ions are transported across the reaction interface[13,16] or it may undergo a heterogeneous mechanism where the oxygen released from the oxidizer would subsequently react with fuel particles.[17,18,19] It has also been suggested that the fuel nanoparticles can have a more violent response under very high heating rates leading to a catastrophic failure of the protective oxide shell and subsequent spallation of the molten fuel.[20] Egan et. al[21] recently conducted experiments of nanoscale Al/CuO composites in a high heating rate transmission electron microscope (Dynamic TEM) and observed the rapid loss of nanostructure to occur about two orders of magnitude

This manuscript was accepted by J. Appl. Phys. Click here to see the version of record.

faster than a heterogeneous reaction, highlighting the dominance of condensed phase reactions at the nanoscale. Other studies, which combine high heating rates and microscopy, have shown, for Al/WO_3[13] and Al/Bi_2O_3,[22] that the loss of nanostructure and the ensuing reaction is limited to regions where there is sufficient contact between the fuel and oxidizer, suggesting a condensed phase initiation. Another recent study[23] that looked at the reaction products of three nanoscale thermite systems highlighted the morphological similarities between the products collected from high heating rate experiments under atmospheric conditions with that of those observed in the Dynamic TEM.[21] The study concluded, through the inspection of the product distribution, that the major contribution to the exothermic reaction occurs through the condensed phase as opposed to a gas phase reaction.

Recent work studying flame propagation of nanothermites[24] has revealed a specialized condition termed 'reactive entrainment' which highlights the prolonged combustion of nanothermites which extend over time scales on the order of milliseconds (≈ 3 ms), displaying a gradual release of energy. This combined with the confined pressure cell data showing initial pressure rise times on the order of 10 μs[25] suggests the possibility of a two-stage combustion where the fast initiation is followed by a slow burning. As the majority of the applications of nanothermites are contingent upon the rapid release of energy feeding the initial pressurization, a quantification of the extent of reaction during the first stage of combustion seems necessary for the development of smart energetics that could be appropriately tuned for maximizing the power output.

The current work is an extension of the previous work on product analysis wherein we tried to identify the predominant energy release pathway in nanothermite reactions.[23] The first part of this work consists of igniting microgram quantities of nanothermites on a resistively heated fine wire followed by rapid quenching and collection of the combustion products, within ≈ 500 μs. This allows us to look at the products formed exclusively during the rapid, first stage of combustion. The extent of oxidation is

This manuscript was accepted by J. Appl. Phys. Click here to see the version of record.

evaluated by employing the focused ion beam (FIB) technique to cross-section the collected product particles, which are subsequently subjected to quantitative elemental analysis using energy dispersive X-Ray spectroscopy (EDX). Three different nanothermite compositions (Al/CuO, Al/WO_3 and Al/Bi_2O_3) are analyzed owing to their diverse combustion characteristics, as discussed in the experimental section. The result obtained from the cross-section analysis is corroborated with the macroscopic heats of reaction for these systems, found using bomb calorimetry. Furthermore, temperature measurements using a spectro-pyrometer were also made to augment the analysis on the extent of reaction.

II. EXPERIMENTAL

A. Materials and Preparation

The composites were chosen to be consistent with those in a previous publication[23] and all three composites exhibit distinctive combustion properties. Jian et. al[26] evaluated reaction phenomena for the three systems at high heating rates (≈ 10^5 K/s) and per their conclusion, Al/CuO nanothermite shows concurrent oxygen release and ignition temperatures in high heating rate experiments, which may entail a gas phase ignition. Al/Bi_2O_3 nanothermite ignites almost 700 K below the oxygen release temperature from the bare oxidizer and it has been subsequently verified that its initiation proceeds through the condensed phase.[22] It is also the most gas producing/ energetic nanothermite of the three studied.[27] Al/WO_3 is believed to undergo a completely condensed phase initiation/ reaction as WO_3 does not release any gas phase oxygen, although it decomposes into gas phase sub-oxides (WO_x) at ≈ 2800 K.[25] The adiabatic temperatures vary with the choice of the thermites, with Al/WO_3 mixtures exhibiting a very high adiabatic flame temperature (3447 K) compared to the Al/CuO formulation (2967 K).[25] Based on the results of Sanders et al.,[12] stoichiometric Al/Bi_2O_3 showed the highest maximum pressure in a closed bomb pressure cell followed by Al/CuO and Al/WO_3. Such variance in combustion performance provides breadth to the current analysis performed in this work.

This manuscript was accepted by J. Appl. Phys. Click here to see the version of record.

Physical mixing of the reactants followed by ultra-sonication is the most common preparation technique for nanothermites and hence, is used in this work. Commercially available aluminum nanoparticles (Argonide Corp.)[†] with an average particle size of 50 nm were used as the fuel. These particles had a core-shell structure with an active aluminum content of 64.5 %, which was confirmed by thermo-gravimetric measurements. The nanoparticles were ultra-sonicated in hexane for approximately 20 min. with three different metal oxide nanopowders. The metal oxide nanopowders used in this study were copper oxide (CuO), tungsten oxide (WO_3), and bismuth trioxide (Bi_2O_3) (all from Sigma Aldrich Corp. and <100 nm) in particle size. A representative scanning electron microscopy (SEM) image of the ultra-sonicated mixtures (Al/Bi_2O_3) can be seen in Figure 1a. A higher magnification image is shown in Figure 1b which highlights the intimate mixing with the brighter areas corresponding to the heavier bismuth trioxide particles and the darker areas corresponding to the lighter aluminum particles (back scattered electron imaging). After ultra-sonication, the intimately mixed nanothermite slurries were micro pipetted onto fine platinum wires for ignition.

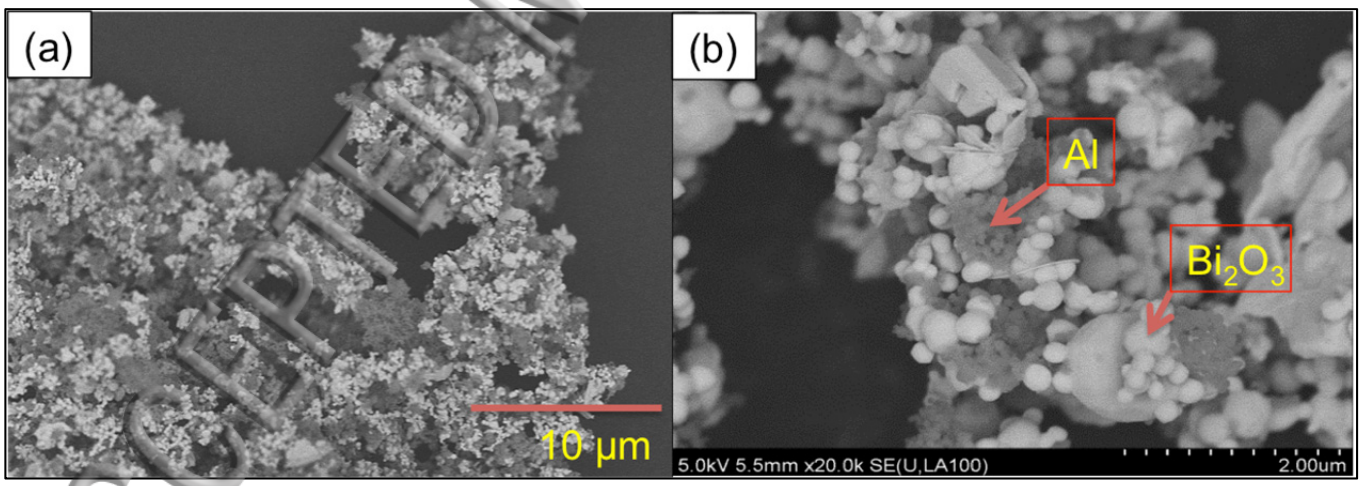

FIG. 1. (a) Precursor (reactant) image of Al/Bi_2O_3 showing the intimate mixing and the elemental contrast owing to the atomic mass of the different reactant species; (b) Higher magnification of the same system as in (a).

[†] Certain commercial equipment, instruments or materials are identified in this paper to foster understanding. Such identification does not imply recommendation or endorsement by the National Institute of Standards and Technology, nor does it imply that the materials or equipment identified are necessarily the best available for the purpose.

This manuscript was accepted by J. Appl. Phys. Click here to see the version of record.

B. Wire Ignition Experimental Setup and Product Collection

The wire ignition experiment consisted of a platinum wire, ≈12 mm length, 76 μm diameter (Omega Engineering Inc.) onto which a slurry of thoroughly mixed nanothermite is coated. The wire is then resistively heated at ≈ 10^5 K/s using a tunable voltage pulse generated by a custom-built power source. The pulse duration was 3 ms and the experiment was conducted in air. The reaction products were collected on an SEM stub (15 mm dia. aluminum, Ted Pella Inc.) which was fixed upon a Z-directional translational stage, allowing the placement of the substrate at various collection distances away from the sample. A layer of carbon tape was attached to the stub so as to improve the sample conductivity under the electron beam. The combustion event was monitored using a high-speed camera (Phantom Miro) from which the approximate transit time for the products before quenching on the stub was calculated. For the current work, the collection stub was placed such that it allowed ≈ 500 μs of transit time for the products before being quenched on the substrate.

C. Dual Beam FIB/SEM

The substrates were subsequently analyzed with focused ion beam scanning electron microscopy (FIB/SEM). The instrument used was a FEI Nova NanoLab 600 DualBeam (Gallium ion source and a Schottky field-emission electron gun) coupled with an 80 mm^2 Oxford X-Max silicon drift detector to do EDX analysis. The primary advantage of the FIB/SEM instrument is the ability to image embedded phases[28], where the high-energy ion beam, upon elastic interaction with the sample, mills the material, revealing the cross-section of the sample. The dual beam system has a vertical electron beam column and a gallium ion beam column tilted at an angle of 52°, both focusing at the same point on the sample. The stage with the sample is first tilted at 52° so as to make it perpendicular to the ion beam and the specimen is subsequently milled. Once the milling is complete, the electron beam is used to image the milled surface as well as obtain elemental spectra (EDX). Obtaining the EDX spectra from a tilted

1 stage has its advantages in that the electron beam enters the sample at an oblique angle, which results
2 in the sample surface absorbing a larger portion of the incident electrons when compared to normal
3 incidence, thereby improving the X-ray emission. However, the stage was not rotated to optimize the
4 take-off angle of X-rays toward the EDX detector from the milled surface and thus the X-ray photon
5 collection was not optimized and longer acquisition times were needed for the analysis.[28] Dual beam
6 FIB/SEM has been extensively used in the semiconductor industry[29] and has found other applications in
7 biological sciences,[30] fuel cells, optical coatings, atmospheric chemistry[28] and primarily TEM sample
8 preparation.[31] Applications of FIB milling in energetics have been limited. FIB assisted nanotomography
9 is a technique that has been used to characterize microstructure and porosity of high explosives to shed
10 more light on the pore collapse mechanism.[32] It has also been used to study intermetallic reactions,[33]
11 synthesis of high explosive composites,[34] as well as examining the extent of oxidation in fine aluminum
12 particles.[35] In this work, we employ the FIB/SEM to mill the product particles of nanothermite reactions
13 so that their interiors can be subjected to quantitative elemental measurements. A representative image
14 of the products on the substrate is shown in Figure 2a. Selected particles are then cross-sectioned using
15 the gallium ion beam, as can be seen in Figure 2b. The cross-section of the sample is subsequently
16 analyzed using the electron beam and the silicon drift detector for elemental quantification.

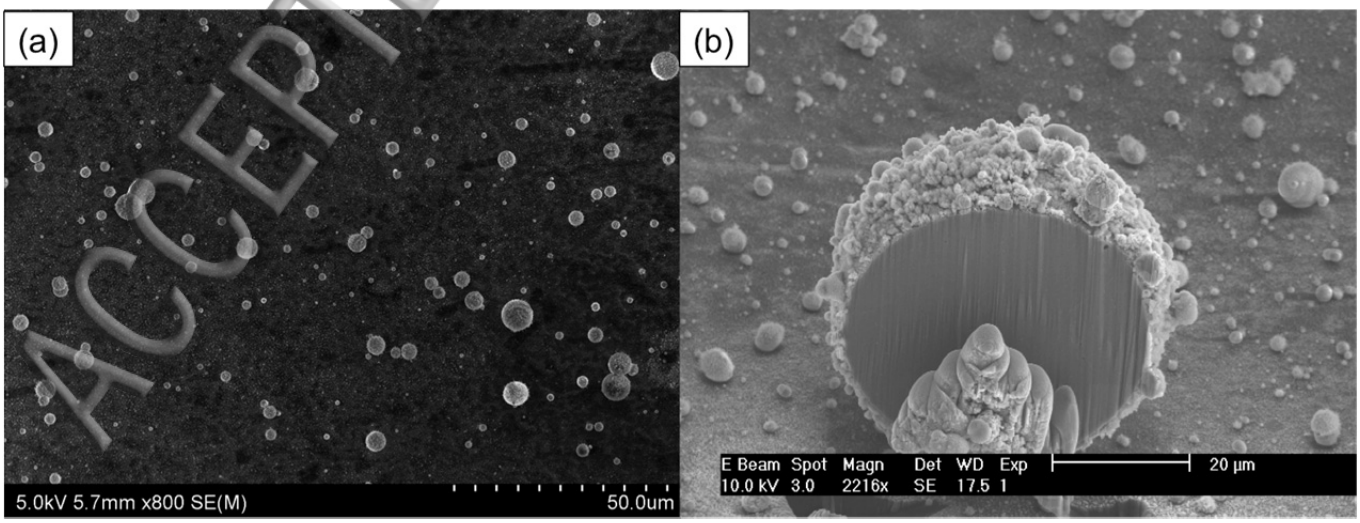

17

FIG. 2. (a) Representative SEM image of products collected for the Al/CuO case; (b) a 20 μm particle sliced using high intensity gallium ion beam.

D. Calorimetry

The micro-calorimeter used in this study is a low heat capacity instrument specially designed for making measurements of small amounts of reactive materials at 1 atm pressure with a choice of ambient gas. The bomb calorimeter is made from titanium and has an inlet valve to adjust the environment and two electrical feed-through pins. Within the bomb, a thin nichrome filament bridges the two electrical pins and is bent to a point and lowered into the sample that is held in a small ceramic crucible (Supplementary Figure S1a-c). The bomb is sealed, vacuum purged twice and filled with 1 atm of argon to ensure a highly inert environment. The bomb is then suspended in a low heat capacity silicone oil that is constantly stirred. To react the sample, a 10 V potential is applied between the electrical pins, causing the filament to heat and ignite the powder in the crucible. The heat from the reaction disperses within the bomb and into the surrounding oil bath, causing the temperature of the entire system to increase by a small amount, as shown in the Supplementary Figure S1d. The total test time was approx. 6 min, with 2 minutes each for three regions of temperature measurement: pre-reaction baseline, temperature rise after ignition, and the post-reaction baseline. The heat of reaction is calculated from the product of the calorimeter constant measured during calibrations (135 J/K) and the temperature rise of the oil bath measured during the experiment. The electrical power from ignition is very small and is subtracted from the calculated heat of reaction. More information about this system can be found in Ref. 36.

E. Spectroscopy and Temperature Measurement

In addition to calorimetry and elemental quantification, temperature measurements during combustion of these nanothermite composites augment the analysis since a reaction temperature closer to the adiabatic flame temperature would suggest a more complete reaction. Given the transient nature of

This manuscript was accepted by J. Appl. Phys. Click here to see the version of record.

the event, the diagnostics used require sub millisecond temporal resolution, which precluded the use of conventional techniques such as thermocouples as well as infrared (IR) cameras. A high-speed 32-channel spectro-pyrometer was built in house which consisted of an optical fiber that collected the light from the reaction zone and transported it into a 0.5 m spectrometer (Acton SP 500i), which dispersed the light using a 150 lines/mm grating. The resulting spectrum was focused onto a 32 channel PMT (Photo Multiplier Tube) array (Hamamatsu H7260) interfaced with a high-speed data acquisition system (Vertilon IQSP 580). PMT based systems have the advantage of extremely fast rise times (≈ 1 ns) along with high dynamic range and sensitivity, which allowed for extremely fast data acquisition. The data was acquired over the wavelength range of 513 nm to 858 nm (incorporating 27 channels of the PMT). The wavelength calibration was done using a HgNe pencil lamp (Newport) and the intensity calibration was done using a calibrated tungsten halogen lamp (Avantes) operated at 2440 K. In this configuration, each channel collected light over a band of wavelengths ≈ 13 nm wide. The sampling rate on the acquisition system was set at 50 kHz, which produced a sample every 20 μs, sufficient to resolve the sub millisecond reactions. The spectrum was subsequently fit to Planck's law, assuming grey body behavior with temperature as a free parameter, to obtain the time-resolved temperature profile.[37] More information regarding the calculation is provided in the supplementary section.

III. Results

A. Stoichiometric Al/CuO Reaction Product Cross-Section

As can be seen in Figure 2, the collected product particle sizes have a wide distribution. However, almost all the product particles seen in the SEM micrograph are two orders of magnitude larger than the nanoscale reactants (50 to 100 nm primaries). Such large products are a direct consequence of coalescence during the rapid exothermic reaction.[13,21] In addition to these large particles, nanosized product populations were also observed on the substrate, which are a result of nucleation from the gas

This manuscript was accepted by J. Appl. Phys. Click here to see the version of record.

phase, although their contribution to the net product mass was previously determined to only be ≈ 10 %.[23] In order to provide sufficient breadth to the analysis, a range of particle sizes (> 1 μm) are considered for ion beam cross-sectioning. Figure 3 shows the cross-sectional view of a ≈ 2 μm diameter product particle, quenched during the combustion of a stoichiometric Al/CuO thermite mixture (ignition temperature: (1040 ± 50) K),[26] accompanied by the area scans. As we can see, there are no visible phase separations within the interior of the particle and the oxygen seems to be evenly distributed throughout the sample.

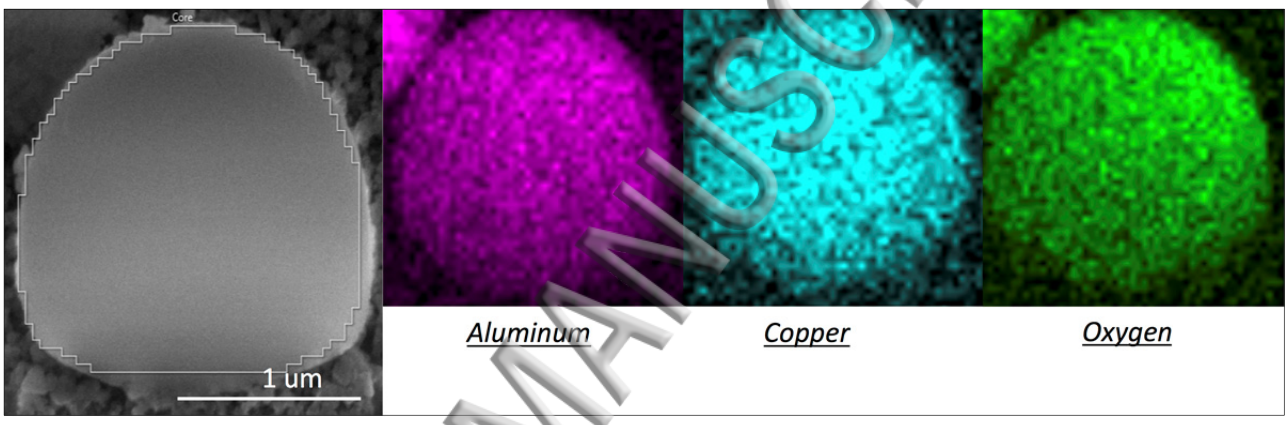

FIG 3. Cross-section SEM image of a ≈2 μm product particle (Al/CuO, ϕ = 1) with the EDX area scans of the associated elements: aluminum (pink), copper (blue), and oxygen (green). Electron beam conditions are 20 keV and 0.62 nA.

Prior to obtaining quantitative data from the EDX spectra, the instrument's calibration was checked using pure, micrometer scale alumina powder (100 μm, Sigma-Aldrich), for which the EDX system quantified the Al:O atomic ratio as 0.64:1 which is close to the expected value of 0.66:1 for pure alumina, implying an accuracy within 3 %. The elemental composition obtained for the sample in Figure 3 is shown in Table 1 along with an average composition obtained for particles of a similar size range (2 to 3 μm). The aluminum to oxygen ratio corresponds to an effective $Al_2O_{2.7}$ composition, which is close to the expected Al_2O_3 from complete oxidation of the fuel. However, several points regarding this conclusion must be clarified. Firstly, since Al_2O_3 is the only known oxide of aluminum in the condensed phase, an effective value of x = 3 in Al_2O_x would imply either a composition of (M + Al_2O_3), where M

This manuscript was accepted by J. Appl. Phys. Click here to see the version of record.

is the reduced metal (Cu in this case) or a mixture of alumina, MO_y and Aluminum, with the Al and MO_y being mixed such that an effective Al_2O_3 composition is obtained. Similarly, if $x > 3$, it would imply that the Al_2O_3 in the product is mixed with another oxide (MO_y) and a $x < 3$ would imply the Al_2O_3 in the product is mixed with some residual aluminum. Secondly, it can be seen from the Al:Cu ratio in Table 1 that the system is significantly aluminum-rich even though the reactants were stoichiometrically mixed.

TABLE I: Atomic %[1] values obtained for the cross-section for different nanothermite systems along with their standard deviations. Equivalence ratio of 1 implies stoichiometrically mixed.

Al/CuO	**Eq. Ratio**	**Al (at %)**	**Cu (at %)**	**O (at %)**	**x in Al_2O_X**	**Al:Cu**
Particle in Fig. 3	1	32	26	42	2.7	1.2
Avg. <5 μm particles (total 5)	1	38 ± 3	21 ± 4	41 ± 3	2.2 ± 0.3	1.9 ± 0.5
Avg. >5 μm (total 3)	1	34 ± 4	36 ± 5	30 ± 1	1.8 ± 0.1	1 ± 0.3
Fuel-rich (Fig. 5b)	1.5	49	14	37	1.5	3.5
Al/WO_3	**Eq. Ratio**	**Al (at %)**	**W (at %)**	**O (at %)**	**x in Al_2O_X**	**Al:W**
Avg. <5 μm particles (total 2)	1	32 ± 0	13 ± 1	55 ± 1	3.4 ± 0	2.4 ± 0.2
Avg. >5 μm (total 2)	1	40 ± 2	13 ± 3	47 ± 1	2.3 ± 0.1	3.2 ± 0.8
Al/Bi_2O_3	**Eq. Ratio**	**Al (at %)**	**Bi (at %)**	**O (at %)**	**x in Al_2O_X**	**Al:Bi**
Avg. <5 μm particles (total 2)	1	42 ± 1	7 ± 3	51 ± 4	2.4 ± 0.2	7 ± 2.4
Avg. >5 μm (total 2)	1	17 ± 1	46 ± 4	37 ± 4	4.4 ± 0.2	0.4 ± 0.1
Theor. Complete Rxn.	**Eq. Ratio**	**Al**	**Reduced metal**	**O**	**x in Al_2O_X**	**Al:M**
Al/CuO	1	27.3	31.7	41	3	0.86
Al/WO_3	1	34.6	13.4	52	3	2.58
Al/Bi_2O_3	1	30.5	23.7	45.8	3	1.29

[1] atomic % from normalized k-ratios

Incorporating the 35.5% weight of the protective oxide shell (estimated via Thermogravimetric Analysis) and assuming complete reduction of copper oxide, the exothermic reaction can be written as

$$2Al + 3CuO + 0.29Al_2O_3 \rightarrow 1.29Al_2O_3 + 3Cu.$$

This corresponds to an Al:Cu ratio of 0.86 in products, which means that the interior of the particle in Figure 3 contains substantially less copper (1.2 vs. 0.86). Calculation of reaction products using the

This manuscript was accepted by J. Appl. Phys. Click here to see the version of record.

NASA CEA[38] equilibrium code gives an adiabatic flame temperature of ≈ 2840 K for the Al/CuO system which is at the boiling point of elemental copper. The calculation predicts a copper vapor mole fraction of 0.29, which theoretically leads to a Al:Cu ratio of 1.41 in the condensed phase, in qualitative agreement with the results in Table I that the reaction products should be aluminum-rich. The vapor phase copper would subsequently nucleate into nanosized particles, but their capture efficiency in our experiment is expected to be low.

A similar analysis is extended to larger particles on the order of 10 μm as shown in Figure 4. There is substantial phase separation in the cross-section of these larger particles. Moreover, several cracks and holes can be seen in the copper-rich region, which suggests the production of gaseous species during sintering. The elemental maps show that oxygen is exclusively found in regions containing aluminum and the effective oxidation in this case is $Al_2O_{1.8}$ as outlined in Table I. This does not imply that the reaction is producing condensed phase AlO, but rather that the product Al_2O_3 is mixed with some residual Aluminum from the reactant, leading to an effective Al:O composition that implies fuel rich, in spite of the reactants being mixed stoichiometrically. What it also means is that at the upper limit, the effective oxidation of the fuel is approximately only 50 % complete in these large particles.

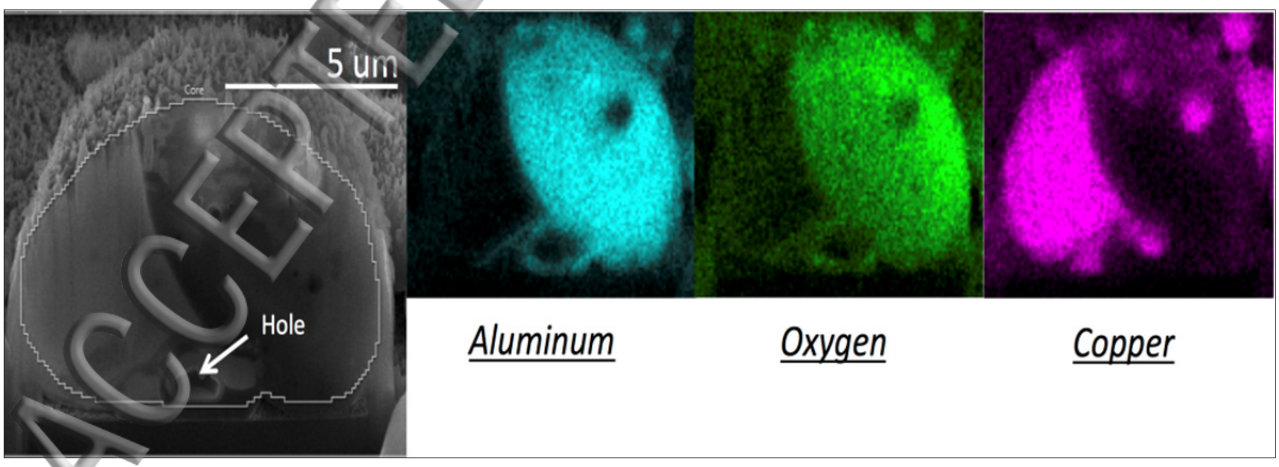

FIG 4. Cross-section SEM image of a 10 μm product particle (Al/CuO, ϕ = 1) with the EDX area scans of the associated elements: aluminum (blue), copper (pink), and oxygen (green). Electron beam conditions are 20 keV and 0.62 nA.

B. Non-Stoichiometric Al/CuO Reaction Product Cross-section

This manuscript was accepted by J. Appl. Phys. Click here to see the version of record.

Similar analysis is extended to Al/CuO thermite mixtures. Two cases were analyzed here: a fuel-lean case with Equivalence ratio (ϕ) = 0.5 and a fuel-rich case with ϕ = 1.5. Figure 5 shows the product cross-sections of non-stoichiometric reactants along with the elemental maps. For the fuel-rich case (Figure 5b), we can see that there is a substantial volume of aluminum with oxygen distributed uniformly throughout the particle. For the aluminum-rich region, an effective composition of $Al_2O_{1.55}$ is obtained which reiterates poor oxidation. This implies that the improved combustion behavior commonly observed at slightly fuel-rich conditions may not be a direct consequence of enhanced oxidation but merely because of the larger amount fuel in the reactants and the improved thermal conductivity which aluminum provides to the reactant mixture.[39] For the case of fuel-lean mixtures, large voids were found within the product cross-sections (Figure 5a) and the elemental maps confirmed that the voids were found in regions with excess copper. The presence of such voids made getting effective Al:O ratio pointless and subsequently we focused more on examining the compositional gradients within the particle. A possible mechanism for the creation of voids could be the un-reduced or partially reduced CuO losing its oxygen during sintering. Given the fuel-lean compositions and the lack of aluminum in the elemental maps, it would be reasonable to assume that the temperature of this particle would have been quite low, thereby making the evaporation of the copper less likely. The presence of oxygen throughout the particle (even in aluminum-lean areas) suggests that some of the oxygen is indeed bonded with copper, which may subsequently be released into the gas phase leading to void formation.

This manuscript was accepted by J. Appl. Phys. Click here to see the version of record.

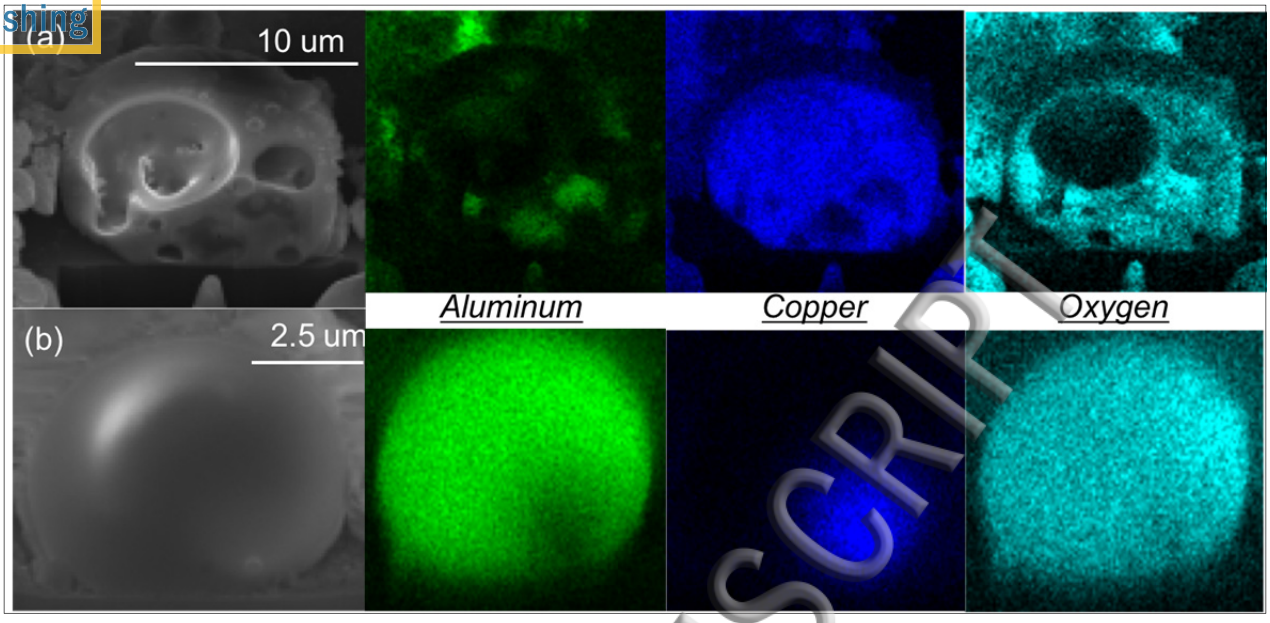

FIG 5. (a) Cross-section SEM image and elemental maps of a 10 μm product particle (Al/CuO, ϕ = 0.5); (b) Cross-section SEM image and elemental maps of a 7 μm product particle (Al/CuO, ϕ = 1.5). Electron beam conditions are 20 keV and 0.62 nA.

C. Stoichiometric Al/WO_3 and Al/Bi_2O_3 Nanothermite Mixtures

Experiments on Al/CuO nanothermite mixtures revealed an enhanced effective oxidation at the smaller product length scales. Copper oxide nanopowder has a high propensity to release gas phase oxygen upon heating,[26] whereas oxidizers like bismuth trioxide and tungsten trioxide show no traces of gas phase oxygen release at temperatures at or below the ignition temperature. Thus it can be expected that upon reaction with aluminum, Bi_2O_3 and WO_3 must show even higher traces of oxygen within the product particles as they are speculated to react solely through the condensed phase. The images for the tungsten and bismuth cases are shown in Figure 6 and the quantitative data shown in Table I reveal higher oxygen content for both cases. Although only a limited amount of data could be obtained for these two thermite systems, the results are in qualitative agreement with the predicted reaction mechanism. For the Al/Bi_2O_3 system, four particles (two per size regime) were analyzed and the proportion of oxygen atoms in Al_2O_X was found to be 2.4 for < 5 μm and 4.4 for > 5 μm particles. The expected Al:Bi ratio for a stoichiometric reaction is 1.29 which implies the smaller particles are

substantially low in bismuth whereas the larger particles seem to be bismuth-rich. Equilibrium calculations predict that most bismuth in the reaction products is in the vapor phase, owing to its low boiling point (1837 K) which could explain the lack of bismuth in the smaller particles. The larger particles, which show substantial amounts of bismuth (Supplementary Figure S3), need a more comprehensive examination since they cannot be formed from the vapor phase coagulation.[23] A visual inspection of the collected products for Al/Bi_2O_3 revealed that the majority of the particles were on the order of a few micrometers. We tried to confirm this observation by performing the image processing routine outlined in Ref. 23 on the electron micrographs of the collected particles. From this analysis, outlined in the Supplementary section, we obtained a qualitative comparison between the product sizes of the three systems. Al//Bi_2O_3 products were the smallest with average particle diameters ranging from 600 nm to 1 μm. This suggests that the large particles found for the Al/Bi_2O_3 case are probably from a region of poor mixing with excessive Bi_2O_3, which might subsequently decompose due to the heat from the adjacent reaction zones. This would also lead to the scenario where $x > 3$ in Al_2O_x which would imply the mixing of aluminum oxide in the reaction product with excess, unreacted/ partially reacted oxide from the reactants.

Similarly, for the Al//WO_3 case, the proportion of oxygen atoms in Al_2O_X was found to vary between 2.3 and 3.4 (Table I) for different particle sizes, which is near the expected value of 3. In both cases the amount of oxygen in the interior was higher than the case of copper oxide and the oxygen was predominantly localized to regions with aluminum. The Al:W ratio vary between 2.4 to 3.2 which is near the predicted value of 2.58, a consequence of barely any gasification. Also, like the copper oxide case, the larger particles contained less oxygen than the smaller ones.

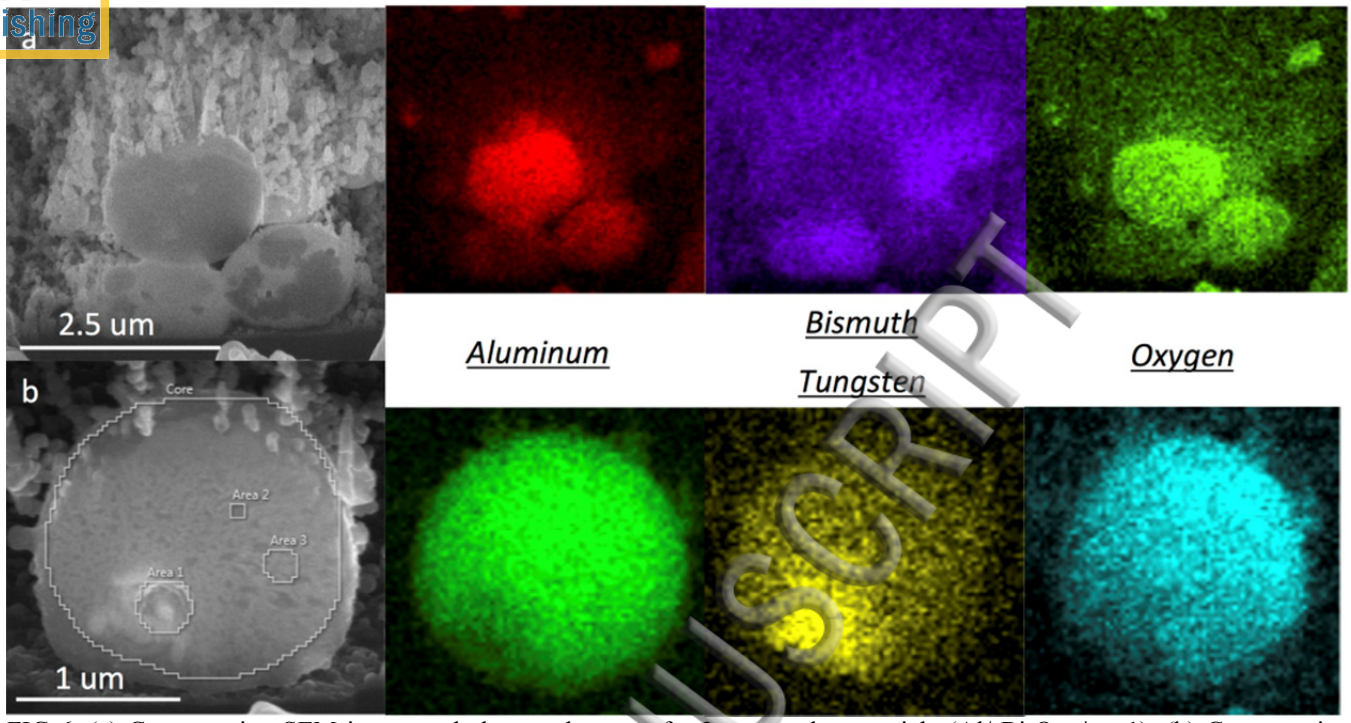

FIG 6. (a) Cross-section SEM image and elemental maps of a 3 μm product particle (Al/ Bi_2O_3, ϕ = 1); (b) Cross-section SEM image and elemental maps of a 2 μm product particle (Al/ WO_3, ϕ = 1). Electron beam conditions are 20 keV and 0.62 nA.

D. Bomb Calorimetry Results

Bomb calorimetry measurements were conducted under argon to prevent any secondary reaction with air. The measured heat of reaction (ΔH_{Rx}), for the three nanothermite systems (stoichiometric), are shown in Table II along with an estimated percentage of completion. The reported average values were obtained from 5 runs of Al/CuO, which helped ensure the repeatability of the experiment and were subsequently extended to Al/WO_3 and Al/Bi_2O_3 (2 runs each). The standard deviations were within 10%, which precluded the need for additional runs for the latter cases.

TABLE II: Bomb calorimetry results for nanothermite reactions along with standard deviations

Thermite (phy.mix)	Exp. ΔH_{Rx} (J/g)	Theo. ΔH_{Rx} (J/g)[1]	% Complete	Gas Prod. @ 101325 Pa (g of gas/g of mix)[40]	Press. Rate (kPa/us)[22,25]	T_{ad} (K)[1]
Al/CuO	2479 ± 334	4071	61	0.343	76.6	2843
Al/WO_3	2192 ± 176	2910	75	0.146	0.2	3253

Al/Bi_2O_3	2141 ± 54	2115	≈100	0.894	108.3	3253

Nanothermite systems reacting via condensed phase mechanism (Al/Bi_2O_3 and Al/WO_3) show higher completion than those having a gas phase reaction component. Literature values for the theoretical gas production, adiabatic flame temperature (T_{ad}) and pressurization rate in constant volume cell tests are also tabulated for further discussion.

E. Reaction Temperature

Reaction temperature was also measured for these nanothermite systems in inert environments (Ar, 1 atm) and the results are shown in Fig. 7a-c along with the adiabatic flame temperature for comparison. Fig. 7d shows high-speed temporal snapshots of the Al/CuO nanothermite reaction, from Fig. 7a, with the time elapsed from trigger shown as insets. The snapshot at 2.882 ms corresponds to the peak temperature observed. Except for the Al/CuO system, the other two nanothermites produce temperatures that are at or below their respective adiabatic flame temperature.

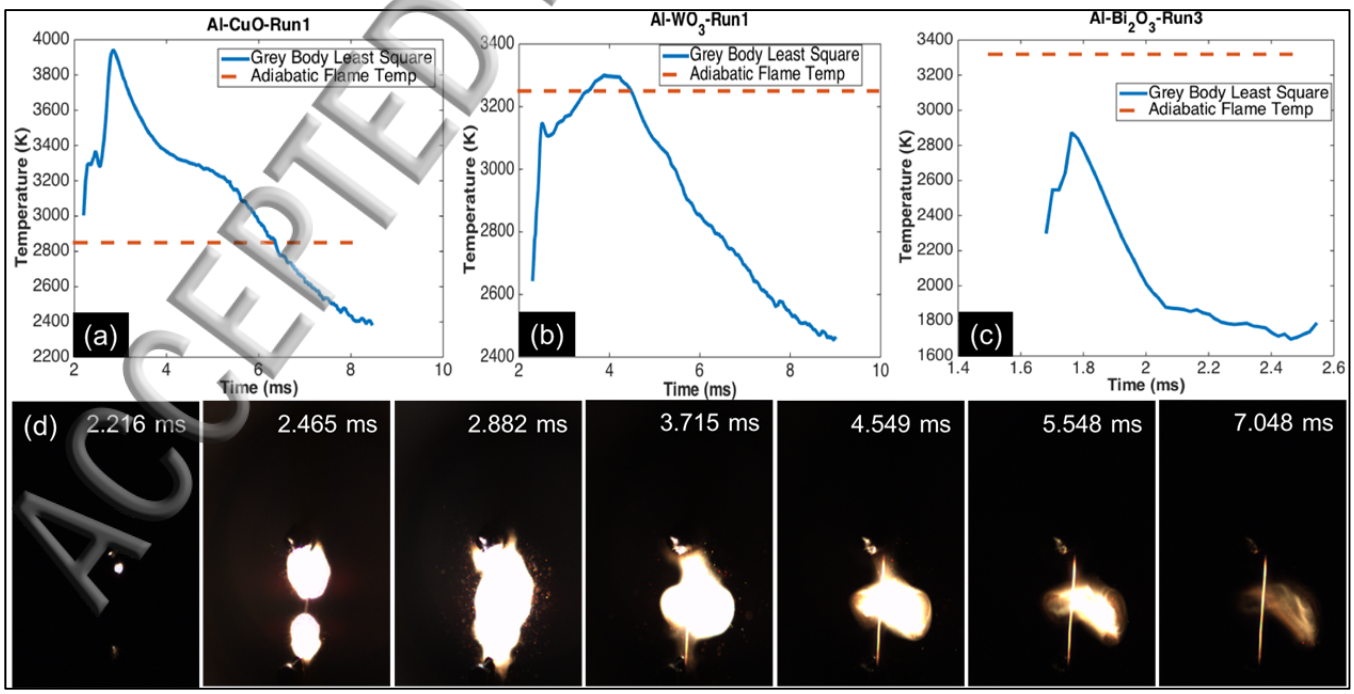

Fig. 7. Temperature profiles in inert environments for (a) Al/CuO, (b) Al/WO_3 and (c) Al/Bi_2O_3; (d) High speed snapshots of Al/CuO reaction on wire shown in (a).

IV. Discussion

The results from the previous section show that the dimensions of the final nanothermite reaction products are on the micrometer scale in spite of the reactants being nanoscale. Molecular dynamics simulations done by Chakraborty et. al[41] have shown that nanoscale aluminum aggregates can lose their surface area and sinter into characteristically larger particles in nanoseconds. Since most nanopowders exist in an agglomerated state, this rapid loss of surface area could be substantial. Experimental validation of this postulate was recently published where temporal snapshots of nanoaluminum aggregates,[42] subjected to high heating rates, were taken in an electron microscope. The results showed that the loss of nanostructure occurred on the order of ≈ 50 ns which is 3 to 4 orders of magnitude faster than the fastest aluminum combustion time observed.[43] The same experiment, extended to Al/CuO nanothermite[21], also showed this rapid loss of nanostructure, occurring on a microsecond timescale. A direct consequence of this loss of nanostructure is the formation of large, condensed phase products[23] which greatly increase the diffusion length scales for the reactants, leading to slow afterburning,[24] thereby defeating the purpose of using nanoscale material for rapid reaction. With this work, we try to examine the detrimental effects of such sintering by quantifying the energy release as well as the internal composition.

The biggest difference between the three nanothermite systems studied here is that in reactions where condensed phase chemistry is predominant (Al/WO_3 and Al/Bi_2O_3), the elemental compositions from the interior revealed a higher oxygen content, implying a higher extent of reaction. This is directly observed on the macroscopic scale as well, in the bomb calorimetry experiments, where larger sample mass and longer sampling duration was employed. The aforementioned nanothermite systems (Al/WO_3 and Al/Bi_2O_3) were observed to approach their theoretical heats of reaction to a greater extent than

This manuscript was accepted by J. Appl. Phys. Click here to see the version of record.

Al/CuO. Moreover, from Table II, it can be seen that the Al/Bi_2O_3 system is expected to produce the most gas phase products upon reaction. This is primarily due to the low boiling point of the bismuth product compared to the other two reduced metals, copper and tungsten. Such excessive gas production could significantly influence the heat of reaction. Firstly, higher gas production could mean a stronger pressure wave emanating from the ignition point which could help in de-aggregating the adjacent reactant particles into smaller clusters, thereby preventing large-scale sintering. Since condensed phase reactions rely on species diffusion, these smaller clusters of fuel and oxidizer would react much faster, owing to their shorter diffusion length scales. This could also lead to the prevention of a two-stage combustion, as outlined earlier, where sintered particles would undergo slow burning in ambient atmosphere.

The influence of gas production on the product sizes was examined further following the procedure in Ref. 23, where image processing, using ImageJ, was performed on the electron micrographs of the collected product. As outlined in the Supplementary section, the electron micrographs of the product particles were converted into a binary greyscale image, which helped in isolating the particles against the background. Once isolated, their effective diameters were calculated from their projected area using the built in algorithm in ImageJ. This helped in obtaining a qualitative comparison between the product sizes of the three systems. Al/Bi_2O_3 products were the smallest with particle diameters ranging from 600 nm to 1 μm. Al/CuO product sizes were approximately 1 μm to 2 μm and Al/WO_3 had product sizes in the 3 μm to 4 μm range. Correlating this observation with that of the gas production, one can see the influence quite clearly with gas production scaling as Al/Bi_2O_3 > Al/CuO > Al/WO_3 leading to product sizes Al/Bi_2O_3 < Al/CuO < Al/WO_3 and reaction completion being Al/Bi_2O_3 > Al/WO_3 > Al/CuO.

The latter correlation for reaction completion does not strictly align with theory of smaller products leading to higher completion. A possible reason for this would be the gas phase oxygen release from

This manuscript was accepted by J. Appl. Phys. Click here to see the version of record.

copper oxide nanopowder, which has been shown to be concurrent with ignition of the Al/CuO nanothermite.[26] This release of oxygen could lead to local asphyxiation of the fuel particles, leading to poor reactivity. This is indeed observed in the spectrometric temperature measurements shown in Fig. 7a, where the initial spike in temperature for the Al/CuO case is near the micrometer aluminum flame temperatures/ alumina volatilization temperatures.[44,45] Since the flame temperatures were measured in an inert environment, the high initial temperature can be explained to be a consequence of a sintered aluminum particle reacting with the gas phase oxygen released from the bare CuO. Such large sintered aluminum aggregates may not completely combust, leading to a drop off in heat of reaction. Moreover, the flame cloud shown in Fig. 7d at 2.882 ms (at the peak temperature shown in Fig. 7a) need not have a homogenous temperature distribution since the spectrometer would be biased to the highest temperature within the cloud (due to intensity being a function of T^4). Hence isolated events of aluminum combustion with ambient oxidizer could be responsible for the high temperature. It should be noted that the measured temperatures for Al/Bi_2O_3 are substantially lower than the adiabatic flame temperature in spite of the reaction going to near completion. A possible reason for this could be that the grey body assumption for temperature calculation fails for this particular reaction due to the highly dilute flame cloud. Recent studies on the effect of emissivity of aluminized flame clouds have suggested that in case of dense particle clouds, multiple scattering could result in an effective grey body behavior.[46] High speed video of the Al/Bi_2O_3 reaction, shown in Supplementary Figure S5, reveals that the flame cloud produced for this system looks less dense compared to those produced for the other two thermites.

Experimental evidence of cracks and voids in the cross-section of the collected products of the oxygen releasing thermites like Al/CuO, suggest that the sintering might be occurring on a time scale much shorter than the gas release. This could be particularly detrimental as the released oxygen would neither support condensed phase nor gas phase oxidation of the fuel. Moreover, this was observed only

This manuscript was accepted by J. Appl. Phys. Click here to see the version of record.

is large particle cross-sections (Fig. 4) and in fuel-lean Al/CuO systems (Fig. 5a), further supporting the claim that smaller products must lead to a more efficient combustion. Several recent experiments have been directed at reducing the product particle size[47,48,43] owing to the higher reactivity that has been observed in cases where there is less coalescence of reactants. Results of Wang et al.[48] showed an increase in the pressurization rate and peak pressure for nanothermite composites that were designed to reduce the coalescence of the reactants through internal gas generation, thereby allowing greater exposure for the fuel to react. Another recent study,[43] which looked at the reactivity of nano aluminum based composites containing gas generators, showed an order of magnitude improvement in reactivity owing to a smaller sized reactant matrix. The underlying principle for all such observations could be explained, based on the current results, as a consequence of reducing the effective diffusion length scales for reactants as well as dispersing the reactants, which would ensure faster reaction and also prevent the unreacted material from getting arrested within a coalesced particle, as seen in Figs. 4 and 5a.

V. Conclusion

Quenched reaction products of thermite systems were analyzed to understand the extent of reaction and energy yield. The product particles were quenched immediately (within 500 μs) upon ignition so as to prevent any adulteration from subsequent reaction with the ambient. The elemental analysis of the product particle cross section revealed that nanothermite compositions where condensed phase reactions are predominant (Al/WO_3 and Al/Bi_2O_3), the elemental compositions from the interior revealed a higher oxygen content, implying a higher extent of reaction. This was correlated on the macroscopic scale as well, in the bomb calorimetry experiments, where the aforementioned nanothermite systems (Al/WO_3 and Al/Bi_2O_3) were observed to approach their theoretical heats of reaction to a greater extent than Al/CuO. The product particle sizes were estimated from the SEM images via image processing and were found to be in the order: Al/Bi_2O_3 < Al/CuO < Al/WO_3. Which

correlated with the total gas release from each nanothermite system (from pressure cell tests) Al/Bi_2O_3 > Al/CuO > Al/WO_3. This implies that strong gas generation during thermite reaction could have a significant effect on inhibiting sintering in the reactants, thereby reducing the length scale that the reactants have to diffuse for reaction in the condensed phase.

The reaction completion, found using bomb calorimetry scaled as Al/Bi_2O_3 > Al/WO_3 > Al/CuO. The lack of correlation between reaction completion and gas generation for the Al/CuO case was interpreted as a consequence of gas phase oxygen release from the bare oxidizer which has been experimentally found to match the ignition temperature. Such release of oxygen gas led to limited oxidizer being present in the condensed phase, which results in poor reactivity observed in calorimetry results as well as lower oxygen content in the elemental maps from cross section. This could also imply that condensed phase reactions are more efficient when it comes overall reactivity since gas phase reactions often occur over longer durations and are plagued by sintering. Furthermore, the results were corroborated with reaction temperature in inert environments where for Al/CuO, significant gas phase reaction between Al and oxygen (released from CuO) was observed ~ 1 ms after ignition. The measured reaction temepratures were at and below the adiabatic flame temepraturs for Al/WO_3 and Al/Bi_2O_3 respectively.

The elemental maps revealed that in all cases, the oxygen was predominantly localized in the regions containing aluminum, although in the case of non-gas-generating thermites, some oxygen could be seen with the reduced metal too. These results imply that the thermite reaction are not be achieving completion even though the constituents are mixed on the nanoscale, owing to severe sintering of the reactants before the reaction can go to completion.

VI. Supplementary Material

Please refer to the supplementary material for schematics and description of the Bomb Calorimeter and Spectro-Pyrometer. Also provided therein are the SEM images and high speed images of the Al/Bi_2O_3 system as well as the image processing routine utilized for product size analysis.

VII. References

1 S. H. Fischer, M. C. Grubelich, and R. I. Iit, Twenty-Fourth International Pyrotechnics Seminar**,** 231 (1998).

2 E. W. Price and R. K. Sigman, Solid Propellant Chemistry, Combustion, and Motor Interior Ballistics **185,** 663 (2000).

3 M. L. Pantoya and J. J. Granier, Propellants Explosives Pyrotechnics **30,** 53 (2005).

4 W. C. Danen and J. A. Martin, (Us Dept Energy (Usat-C) Us Dept Energy (Usat-C)).

5 C. E. Aumann, G. L. Skofronick, and J. A. Martin, Journal of Vacuum Science & Technology B **13,** 1178 (1995).

6 K. S. Martirosyan, L. Wang, and D. Luss, Chemical Physics Letters **483,** 107 (2009).

7 R. Thiruvengadathan, A. Bezmelnitsyn, S. Apperson, C. Staley, P. Redner, W. Balas, S. Nicolich, D. Kapoor, K. Gangopadhyay, and S. Gangopadhyay, Combustion and Flame **158,** 964 (2011).

8 R. J. Jacob, B. R. Wei, and M. R. Zachariah, Combustion and Flame **167,** 472 (2016).

9 A. Prakash, A. V. McCormick, and M. R. Zachariah, Nano Letters **5,** 1357 (2005).

10 T. M. Tillotson, A. E. Gash, R. L. Simpson, L. W. Hrubesh, J. H. Satcher, and J. F. Poco, Journal of Non-Crystalline Solids **285,** 338 (2001).

11 J. Kwon, J. M. Ducere, P. Alphonse, M. Bahrami, M. Petrantoni, J.-F. Veyan, C. Tenailleau, A. Esteve, C. Rossi, and Y. J. Chabal, Acs Applied Materials & Interfaces **5,** 605 (2013).

12 V. E. Sanders, B. W. Asay, T. J. Foley, B. C. Tappan, A. N. Pacheco, and S. F. Son, Journal of Propulsion and Power **23,** 707 (2007).

13 K. T. Sullivan, W. A. Chiou, R. Fiore, and M. R. Zachariah, Applied Physics Letters **97** (2010).

14 G. C. Egan and M. R. Zachariah, Combustion and Flame **162,** 2959 (2015).

15 S. F. Son, B. W. Asay, T. J. Foley, R. A. Yetter, M. H. Wu, and G. A. Risha, Journal of Propulsion and Power **23,** 715 (2007).

16 G. Jian, N. W. Piekiel, and M. R. Zachariah, Journal of Physical Chemistry C **116,** 26881 (2012).

17 L. Zhou, N. Piekiel, S. Chowdhury, and M. R. Zachariah, Journal of Physical Chemistry C **114,** 14269 (2010).

18 S. Zhang and E. L. Dreizin, Journal of Physical Chemistry C **117,** 14025 (2013).

19 W. Zhou, J. B. DeLisio, X. Wang, G. C. Egan, and M. R. Zachariah, Journal of Applied Physics **118,** 114303 (2015).

20 V. I. Levitas, M. L. Pantoya, and S. Dean, Combustion and Flame **161,** 1668 (2014).

21 G. C. Egan, T. LaGrange, and M. R. Zachariah, Journal of Physical Chemistry C **119,** 2792 (2015).

22 N. W. Piekiel, L. Zhou, K. T. Sullivan, S. Chowdhury, G. C. Egan, and M. R. Zachariah, Combustion Science and Technology **186,** 1209 (2014).

23 R. J. Jacob, G. Jian, P. M. Guerieri, and M. R. Zachariah, Combustion and Flame **162,** 258 (2015).

24 K. T. Sullivan, O. Cervantes, J. M. Densmore, J. D. Kuntz, A. E. Gash, and J. D. Molitoris, Propellants Explosives Pyrotechnics **40,** 394 (2015).

25 K. Sullivan and M. R. Zachariah, Journal of Propulsion and Power **26,** 467 (2010).

26 G. Q. Jian, S. Chowdhury, K. Sullivan, and M. R. Zachariah, Combustion and Flame **160,** 432 (2013).

27 K. S. Martirosyan, Journal of Materials Chemistry **21,** 9400 (2011).

28 J. M. Conny, Environmental Science & Technology **47,** 8575 (2013).

29 F. Altmann and R. J. Young, Journal of Micro-Nanolithography Mems and Moems **13** (2014).

30 K. Grandfield and H. Engqvist, Advances in Materials Science and Engineering (2012).

31 M. W. Phaneuf, Micron **30,** 277 (1999).

32 R. R. Wixom, A. S. Tappan, A. L. Brundage, R. Knepper, M. B. Ritchey, J. R. Michael, and M. J. Rye, Journal of Materials Research **25,** 1362 (2010).

33 C. E. Shuck, M. Frazee, A. Gillman, M. T. Beason, I. E. Gunduz, K. Matous, R. Winarski, and A. S. Mukasyan, Journal of Synchrotron Radiation **23,** 990 (2016).

34 H. W. Qiu, V. Stepanov, T. M. Chou, A. Surapaneni, A. R. Di Stasio, and W. Y. Lee, Powder Technology **226,** 235 (2012).

35 B. Rufino, F. Boulc'h, M. V. Coulet, G. Lacroix, and R. Denoyel, Acta Materialia **55,** 2815 (2007).

36 K. R. Overdeep and T. P. Weihs, Journal of Thermal Analysis and Calorimetry **122,** 787 (2015).

37 D. Ng and G. Fralick, Review of Scientific Instruments **72,** 1522 (2001).

38 B. J. McBride and S. Gordon, "Computer Program for Calculation of Complex Chemical Equilibrium Compositions and Applications II. User's Manual and Program Description," (1996).

39 J. J. Granier and M. L. Pantoya, Combustion and Flame **138,** 373 (2004).

40 J. A. Puszynski, C. J. Bulian, and J. J. Swiatkiewicz, Journal of Propulsion and Power **23,** 698 (2007).

41 P. Chakraborty and M. R. Zachariah, Combustion and Flame **161,** 1408 (2014).
42 G. C. Egan, K. T. Sullivan, T. LaGrange, B. W. Reed, and M. R. Zachariah, Journal of Applied Physics **115** (2014).
43 R. J. Jacob, B. Wei, and M. R. Zachariah, Combustion and Flame (2015).
44 P. Bucher, R. A. Yetter, F. L. Dryer, T. P. Parr, and D. M. Hanson-Parr, Twenty-Seventh Symposium (International) on Combustion, Vols 1 and 2**,** 2421 (1998).
45 P. Lynch, H. Krier, and N. Glumac, Combustion and Flame **159,** 793 (2012).
46 P. Lynch, H. Krier, and N. Glumac, Journal of Thermophysics and Heat Transfer **24,** 301 (2010).
47 T. R. Sippel, S. F. Son, and L. J. Groven, Combustion and Flame **161,** 311 (2014).
48 H. Wang, G. Jian, G. C. Egan, and M. R. Zachariah, Combustion and Flame **161,** 2203 (2014).

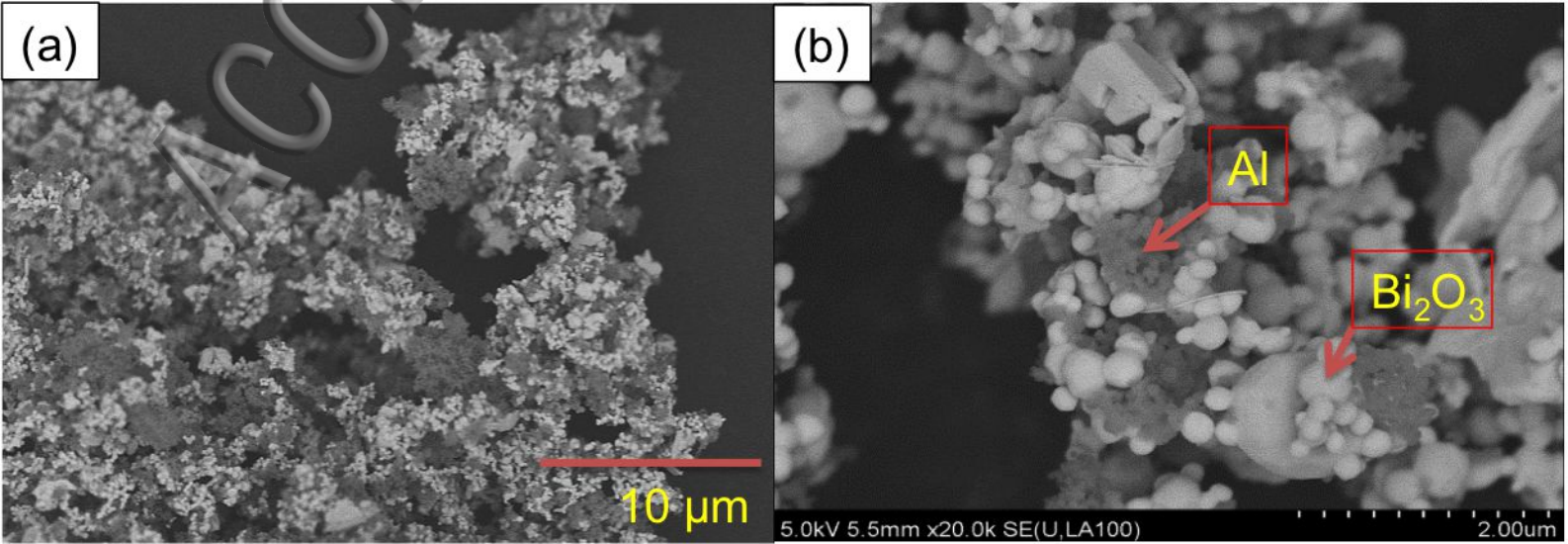
(a)
10 μm
(b)
Al
Bi_2O_3
5.0kV 5.5mm x20.0k SE(U,LA100)
2.00um

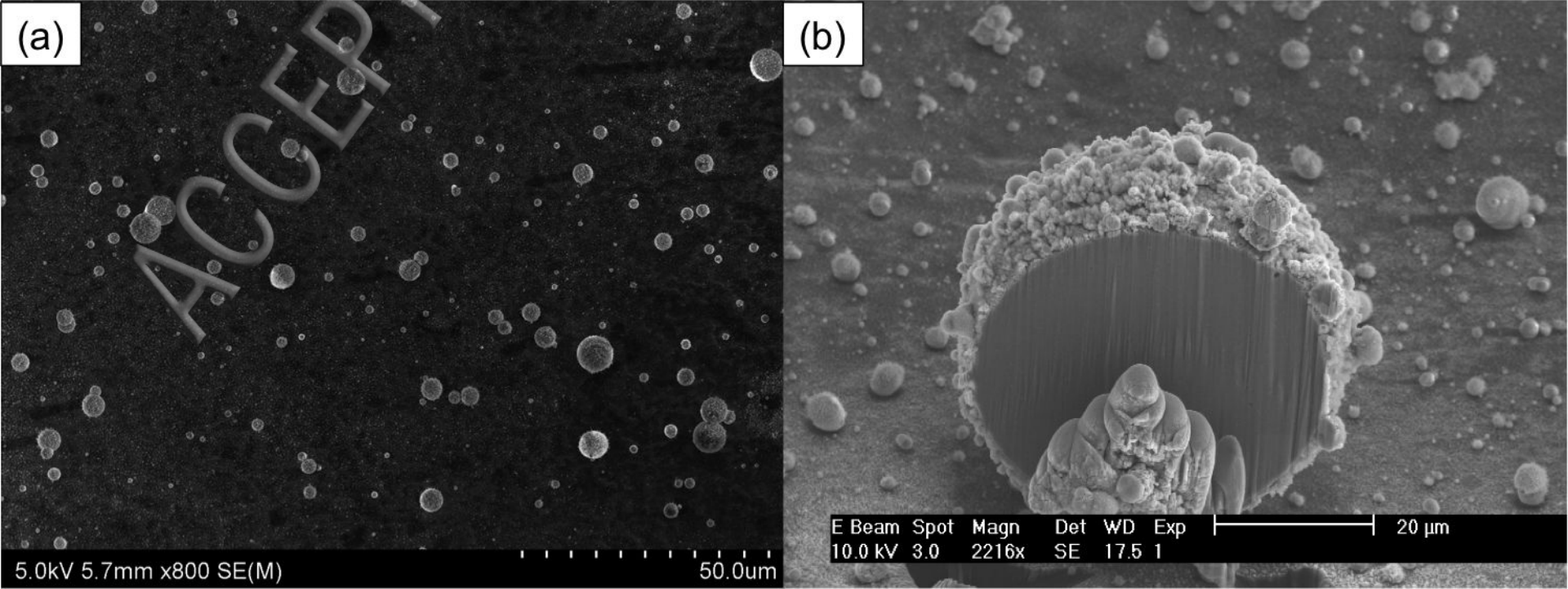
(a)
5.0kV 5.7mm x800 SE(M)
50.0um
(b)
E Beam Spot Magn Det WD Exp
10.0 kV 3.0 2216x SE 17.5 1
20 µm

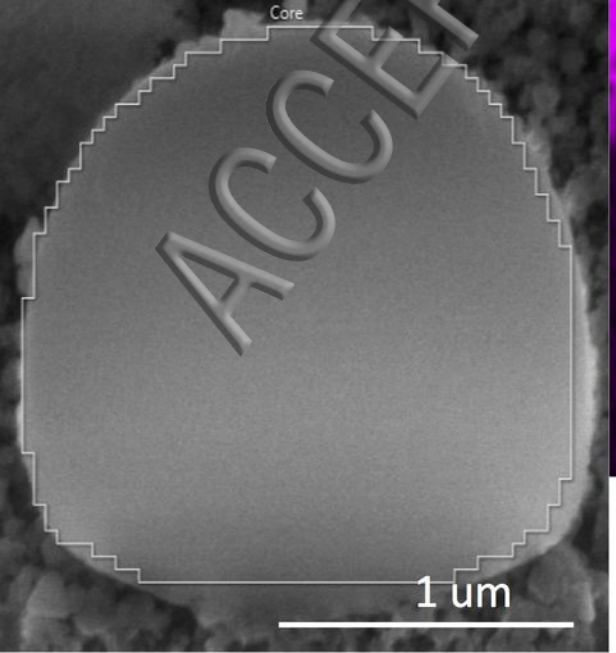

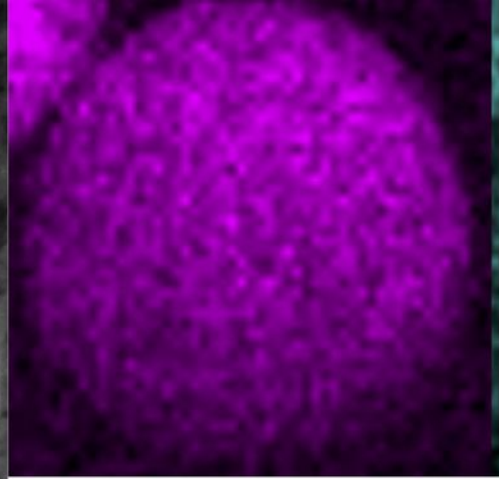

Aluminum

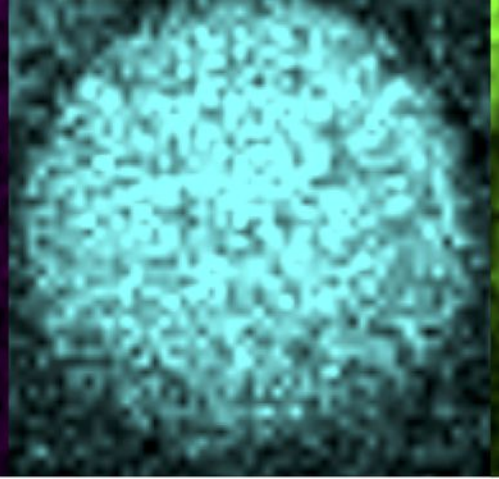

Copper

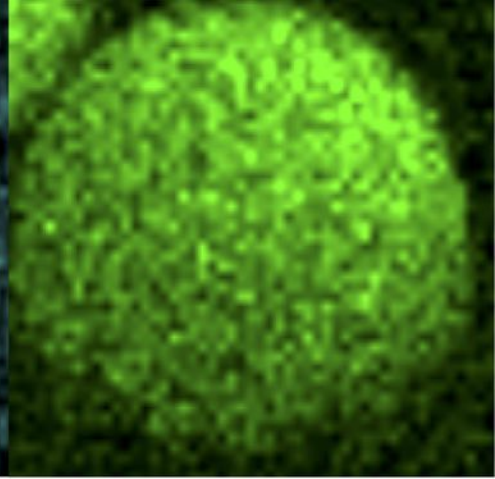

Oxygen

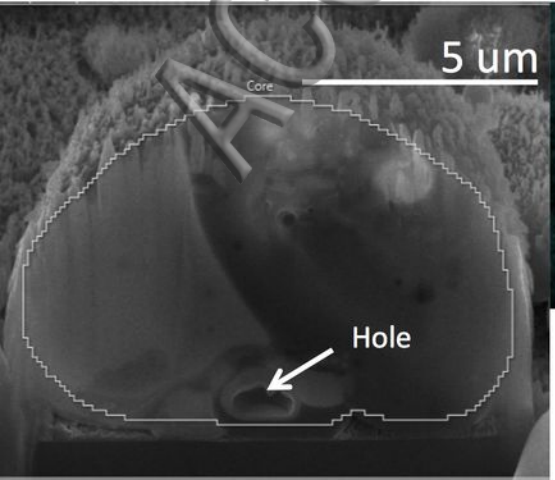

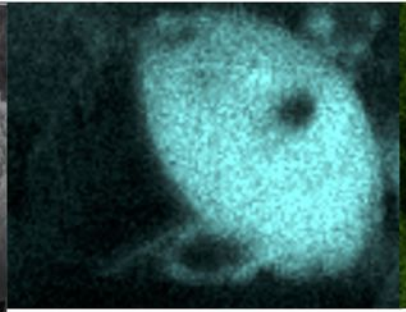

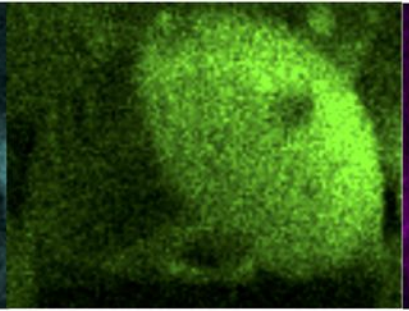

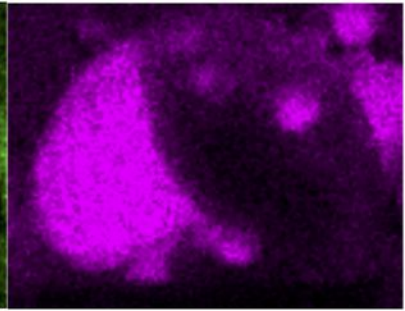

Aluminum *Oxygen* *Copper*

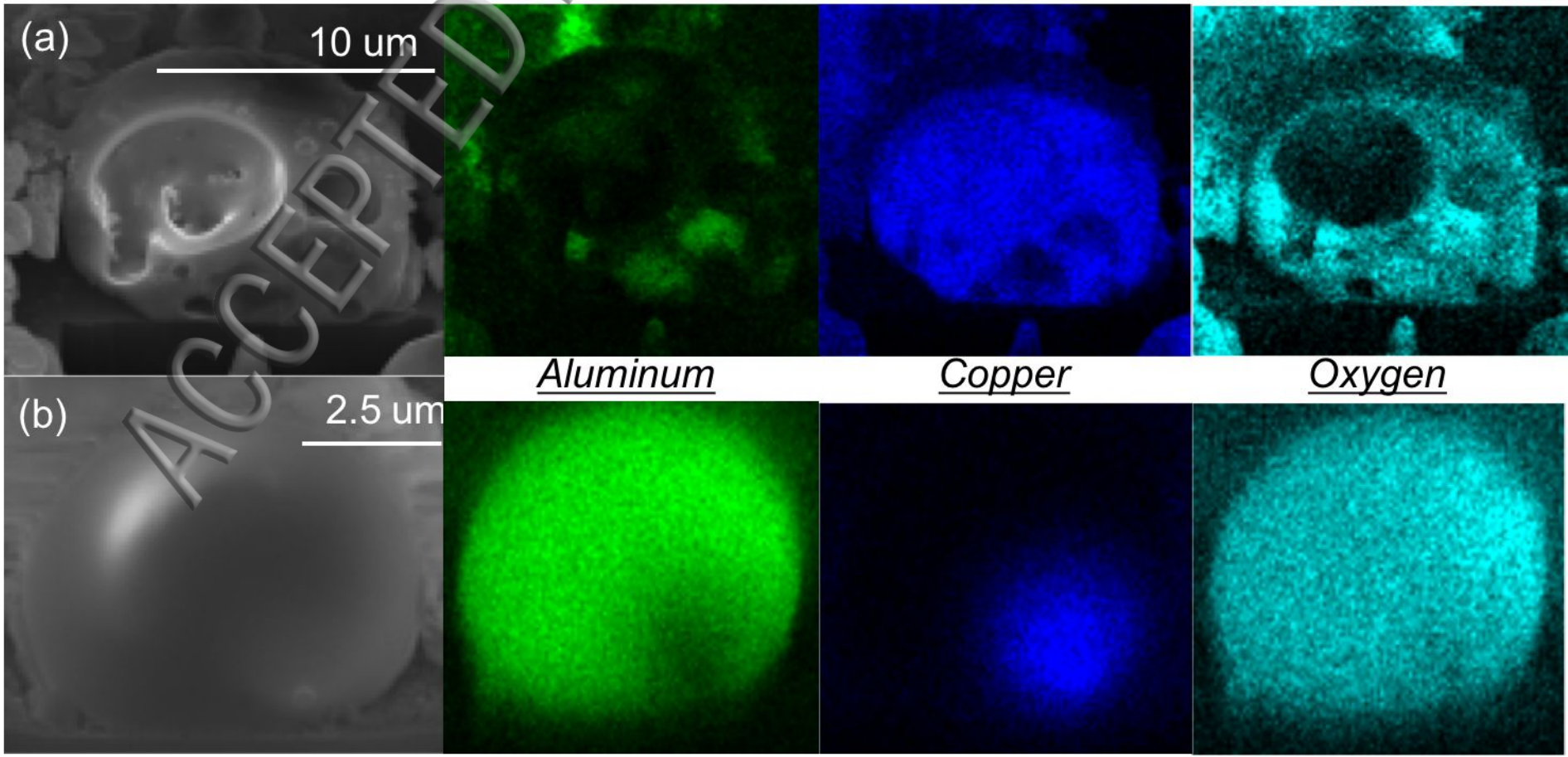

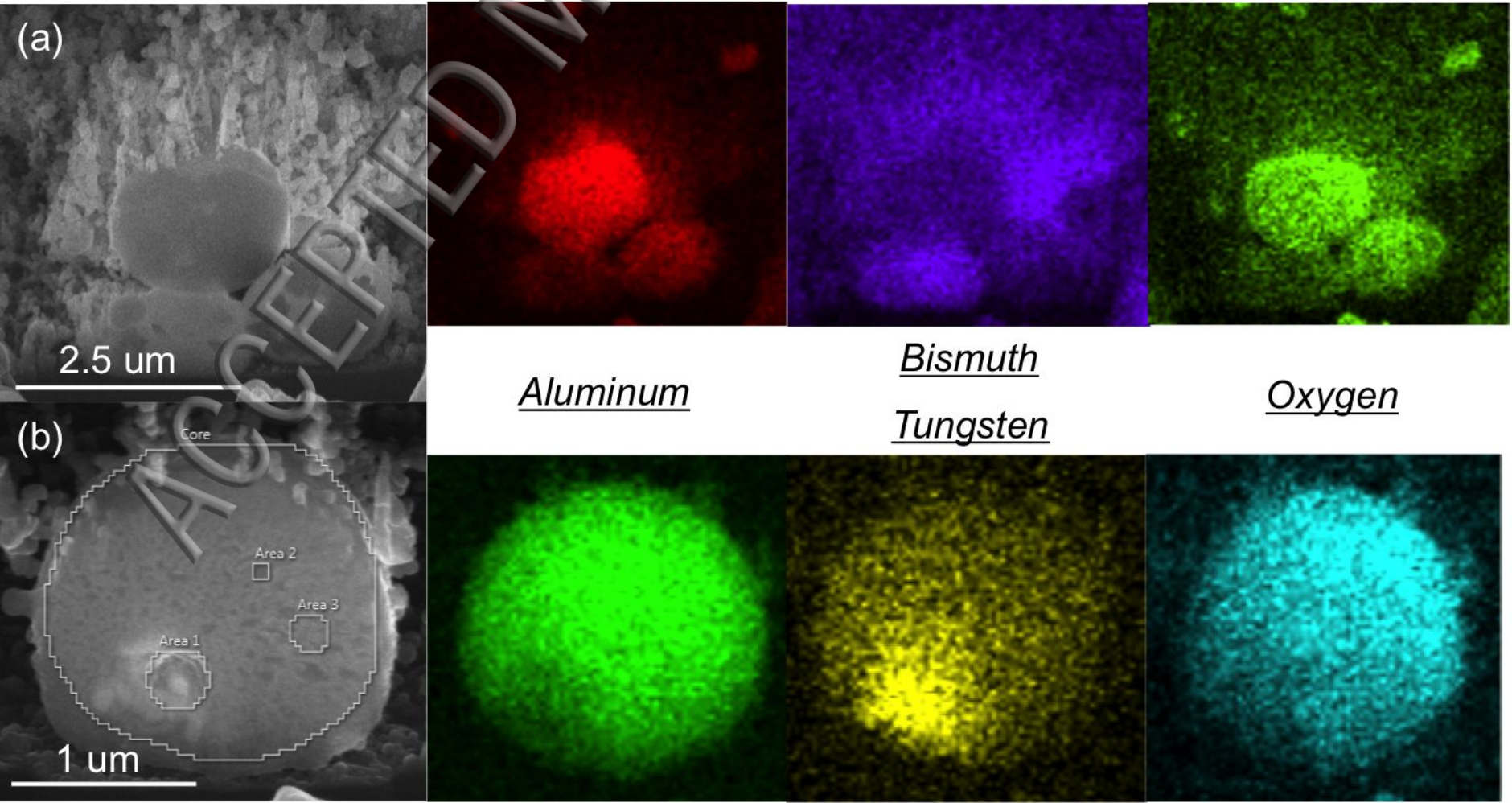
(a)
2.5 um
(b)
Core
Area 2
Area 3
Area 1
1 um
Aluminum
Bismuth
Tungsten
Oxygen